




Article

CoM-ZSM5 (M = Zn and Ni) Zeolites for an Oxygen Evolution Reaction in Alkaline Media

Jadranka Milikić^{1,*}, Srna Stojanović¹, Katarina Rondović¹, Ljiljana Damjanović-Vasilić^{1,*}, Vladislav Rac²
and Biljana Šljukić^{1,3}

¹ Faculty of Physical Chemistry, University of Belgrade, Studentski trg 12-16, 11158 Belgrade, Serbia; srna@ffh.bg.ac.rs (S.S.); katarina.rondovic@ffh.bg.ac.rs (K.R.); biljka@ffh.bg.ac.rs or biljana.paunkovic@tecnico.ulisboa.pt (B.Š.)

² Faculty of Agriculture, University of Belgrade, Nemanjina 6, 11080 Belgrade, Serbia; vladarac@agrif.bg.ac.rs

³ Center of Physics and Engineering of Advanced Materials, Laboratory for Physics of Materials and Emerging Technologies, Chemical Engineering Department, Instituto Superior Técnico, Universidade de Lisboa, 1049-001 Lisbon, Portugal

* Correspondence: jadranka@ffh.bg.ac.rs (J.M.); ljiljana@ffh.bg.ac.rs (L.D.-V.)

Abstract: An ion-exchange procedure of synthetic zeolite ZSM-5 (Si/Al = 15) was used to prepare three cobalt ZSM-5 zeolites (CoM-ZSM5 (M = Zn and Ni)) that were examined for OERs in alkaline media. The structural, morphological, and surface properties of the prepared materials were studied by X-ray powder diffraction, Fourier transform infrared spectroscopy, scanning electron microscopy with energy dispersive spectroscopy, and low-temperature nitrogen adsorption. All three electrocatalysts showed OER activity where CoNi-ZSM5 presented the highest current density (9.5 mA cm⁻² at 2 V), the lowest Tafel slope (134 mV dec⁻¹), and the lowest resistances of the charge transfer reaction (31.5 Ω). Overpotential (η_{onset}) at an onset potential of 410 mV for both CoNi-ZSM5 and Co-ZSM5 and 440 mV for CoZn-ZSM5 electrodes was observed. Co-ZSM5 showed somewhat lower OER catalytic activity than CoNi-ZSM5, while CoZn-ZSM5 demonstrated the lowest OER catalytic activity. The R_{ct} of CoZn-ZSM5 is significantly higher than the R_{ct} of CoNi-ZSM5, which could lead to their different OER activities. Good OER stability and low price are the main advantages of the synthesized CoM-ZSM5 samples in this study.



Citation: Milikić, J.; Stojanović, S.; Rondović, K.; Damjanović-Vasilić, L.; Rac, V.; Šljukić, B. CoM-ZSM5 (M = Zn and Ni) Zeolites for an Oxygen Evolution Reaction in Alkaline Media. *Processes* **2024**, *12*, 907. <https://doi.org/10.3390/pr12050907>

Academic Editor: Qunjie Xu

Received: 5 April 2024

Revised: 27 April 2024

Accepted: 28 April 2024

Published: 29 April 2024



Copyright: © 2024 by the authors. Licensee MDPI, Basel, Switzerland. This article is an open access article distributed under the terms and conditions of the Creative Commons Attribution (CC BY) license (<https://creativecommons.org/licenses/by/4.0/>).

Keywords: ZSM-5 zeolite; water electrolysis; oxygen evolution reaction; bimetal electrocatalyst; transition metal electrocatalyst

1. Introduction

Among the most popular electrochemical devices in the recent decades is an electrochemical water-splitting device (EWS), which presents the most efficient way to produce oxygen (O₂) and hydrogen (H₂) by oxygen evolution reaction (OER) and hydrogen evolution reaction (HER), respectively [1]. The efficiency of these devices mainly depends on electrocatalysts used for both reactions, especially for OER because of its sluggish kinetics via the transfer of four electrons [1]. It is common knowledge that the oxides of precious metals (iridium oxide (IrO₂) and ruthenium oxide (RuO₂)) are the most active electrocatalysts due to their low overpotential and high OER rates with good stability [1–4]. On the other hand, their high prices and scarcity limit their use for widely commercial applications [1–4]. One of the solutions could be preparing these precious electrocatalysts with a reduced amount of Ir and Ru [5,6] or preparing precious metal-free electrocatalysts, such as transition metals (TMs) electrocatalysts [1,4,7–9], TM oxides [1,2,7], and TM sulfides [2,10].

Different types of zeolites exchanged or doped with TMs were examined for OERs [11–17]. Four samples of cerium-exchanged zeolites, synthetic 13X, and natural clinoptilolite (Ce-13X cal, Ce-13X, Ce-Cl cal, and Ce-Cl) were prepared and investigated for OERs in alkaline media [13]. Ce-13X cal showed the highest OER current and the lowest onset potential (1.60 V) [13]. ZSM-5

and β zeolites were ion-exchanged with cerium and calcined to prepare four different OER electrocatalysts (Ce-ZSM-5 cal, Ce-ZSM-5, Ce- β , and Ce- β cal) [16]. In this case, Ce- β cal demonstrated the highest OER catalytic activity showing the highest current density and the lowest Tafel slope (114 mV dec⁻¹) in 1 M KOH [16]. Additionally, NiA and NiX zeolites showed OER activity in alkaline media [11]. NiA showed higher OER activity because of a higher amount of Ni than in the NiX sample [11]. 13X zeolite and an aniline monomer in nickel foam were used to synthesize 13X/PANI-10, -15, -20, and -25 electrodes by electropolymerization and tested for OERs [12]. A Tafel slope of 168 mV dec⁻¹ was obtained for 13X/PANI-15 [12]. A bimetal porous zeolite imidazole framework carbon-based electrocatalyst of a Mo_{0.84}Ni_{0.16}-Mo₂C@NC nanosphere was synthesized by hydrothermal treatment and tested for OER in alkaline media [14]. Mo_{0.84}Ni_{0.16}-Mo₂C@NC showed high OER activity with a current density close to 100 mA cm⁻² at ~1.7 V and a low Tafel slope of 60 mV dec⁻¹ [14].

ZSM-5 (Zeolite Socony Mobil No. 5) zeolite, composed of 96 TO₄ tetrahedra (T = Si, Al) that form a three-dimensional network, is the most investigated zeolite because of its vast industrial applications [18]. The crystalline structure of inorganic ZSM-5 zeolite is built of zigzag 10-membered ring channels (5.1 Å × 5.5 Å) connected with other 10-membered ring channels (5.3 Å × 5.6 Å) that are perpendicular to each other, with a channel intersection size of ca. 8.5–9.0 Å [19]. The microporosity of ZSM-5 zeolite, a high specific surface area, and well-defined pores and channels [20] have also led to its wide investigation for energy storage purposes [21–24]. One of the typical features of zeolites is the ability to easily exchange cations that are located in their pores at specific sites. This can be used to modify the characteristics of zeolites that are influenced by the type, number, and location of extra-framework cations. Hence, simple ion-exchange procedures can be used to introduce electroactive metal centers in zeolitic structures. The cation-exchange capacity of zeolites presents the amount of exchangeable cations, and it increases with a decreasing Si/Al ratio. Synthetic aluminosilicate zeolites usually compensate for the negative charge of the zeolitic framework with NH₄⁺, alkaline, or earth alkaline metals, which can be exchanged by cations of transition metals [25]. Thus, inexpensive zeolite-based electrodes can be prepared by the aqueous ion exchange of zeolites.

The aim of this work was to obtain mono- and bimetallic electroactive catalysts based on ZSM-5 zeolite. Three different CoM-ZSM5 (M = Zn and Ni) zeolites were prepared, characterized by scanning electron microscopy with energy dispersive spectroscopy (SEM-EDS), Fourier transform infrared (FTIR) spectroscopy, X-ray powder diffraction (XRPD), and low-temperature nitrogen adsorption, and were investigated in detail for OER in alkaline media. OER measurements of CoM-ZSM5 electrodes were performed by cyclic voltammetry (CV), linear sweep voltammetry (LSV), electrochemical impedance spectroscopy (EIS), and chronoamperometry (CA).

2. Materials and Methods

The materials investigated in this work were prepared from the hydrogen form of synthetic zeolite ZSM-5 (Si/Al = 15) bought from Zeolyst, denoted in this work as ZSM5. An ion-exchange procedure was accomplished in the diluted aqueous solution of divalent salt: 5 g of ZSM-5 zeolite was stirred for 7 days at room temperature in 1 L of a 0.003 M Co(NO₃)₃ × 6H₂O (purity ≥ 98%, Fluka) solution, then filtered, rinsed with deionized water, and dried for two hours at 80 °C in air.

The bimetallic sample was prepared by mixing 2 g of cobalt-exchanged ZSM-5 zeolite and 400 mL of a 0.003 M solution of Zn(NO₃)₂ × 6H₂O (purity ≥ 98%, Fluka) on a magnetic stirrer for 7 days, at room temperature. The obtained bimetallic CoZn-ZSM5 sample was filtered, rinsed with deionized water, and dried for two hours at 80 °C in air. The same procedure was performed for the aqueous ion exchange of cobalt-exchanged ZSM-5 zeolite with a 0.003 M solution of Ni(NO₃)₂ × 6H₂O (purity 99%, Merck).

All ion-exchanged zeolites were calcined at 500 °C for 5 h in air and denoted as Co-ZSM5, CoZn-ZSM5, and CoNi-ZSM5.

The characterization of all materials investigated in this work was performed using the following experimental techniques. X-ray powder diffraction (XRPD) patterns were used for the investigation of the crystallinity of prepared materials that were obtained with a Rigaku Ultima IV diffractometer in Bragg–Brentano geometry by Cu K α radiation ($\lambda = 1.54178 \text{ \AA}$, from 4° to 50° 2θ in a 0.020° step with an acquisition rate of $1^\circ/\text{min}$).

A Thermo Nicolet Avatar 370 spectrometer in a wavenumber range from 4000 cm^{-1} to 400 cm^{-1} using the KBr pellets technique, with a 4 cm^{-1} resolution and 64 acquisitions was used for collecting Fourier transform infrared (FTIR) spectra. The results were used to study the structural features of the investigated zeolites.

Morphological characterization was performed using a Tescan Mira 3 XMU field emission scanning electron microscope (FESEM). Before the FESEM analysis, the powders were coated with Cu using a CY-PSP180G-1TA plasma-coated sputtering apparatus from Zhengzhou CY Scientific. An energy dispersive spectrometer (EDS) equipped with an INCA x-act X-ray detector and Aztec 4.3 software package (Oxford Instruments, UK), coupled to TESCAN Mira3 XMU, was used for elemental analysis. The applied acceleration voltage was 20 kV. A minimum of three areas of $190 \times 190 \mu\text{m}^2$ were analyzed on each sample to obtain a representative composition.

The surface area and porosity measurements of the obtained samples were performed by a Microtrac Belsorp Mini X instrument. Before the analysis, zeolites were degassed under vacuum for 2 h at 400°C (heating rate $1^\circ/\text{min}$). The textural parameters were calculated from N_2 adsorption–desorption isotherms using Brunauer–Emmett–Teller (BET), t-plot, and Barrett, Joyner, and Halenda (BJH) methods.

All electrochemical measurements were performed using an Ivium V01107 Potentiostat/Galvanostat. A graphite rod and saturated calomel electrode (SCE) were set as counter and reference electrodes, respectively. All potentials in this study are presented versus the reversible hydrogen electrode (RHE). Three CoM-ZSM5 electrodes were set as working electrodes. The catalytic ink-preparation procedure is presented in ref. [16]. Namely, 5 and 0.6 mg of the powder and Vulcan XC-72R, respectively, were ultrasonically mixed in $20 \mu\text{L}$ of a 2% polyvinylidene difluoride solution in N-methyl-2-pyrrolidone (PVDF) for 30 min. Because of the low electric conductivity of the zeolites [26], Vulcan XC-72R was added to increase the electric conductivity of CoM-ZSM5 electrocatalysts. Before pipetting the catalytic ink, the glassy carbon tip was cleaned with ultrapure water in an ultrasonic bath for several minutes. Then, $10 \mu\text{L}$ of the prepared catalytic ink was pipetted onto a cleaned glassy carbon tip to prepare the working electrode, which, afterward, was dried for 12 h at 100°C . A geometrical surface area of the glassy carbon tip (0.945 cm^2) was used for calculating the current densities presented in this work.

A cyclic voltammetry (CV) investigation in an N_2 -saturated 1 M KOH solution at different scan rates ranging from 10 to 100 mV s^{-1} was performed for the calculation of double-layer capacitance (C_{dl}).

The investigation of CoM-ZSM5 (M = Zn and Ni) zeolites' activity for OER was performed by linear sweep voltammetry (LSV) in a 1 M KOH solution at 20 mV s^{-1} . Stability tests were completed at 1.9 V for 3600 s by chronoamperometry (CA). Electrochemical impedance spectroscopy (EIS) measurements with three electrodes were performed in the frequency range of 100 kHz to 0.1 Hz, with a 5 mV amplitude.

3. Results

3.1. Characterization of CoM-ZSM5 Electrocatalysts

X-ray powder diffraction analysis was used to investigate the crystallinity of parent and ion-exchanged zeolites, as shown in Figure 1, because the ion-exchange procedure can modify zeolite structure.

The XRD patterns of Co-ZSM5, as well as CoZn-ZSM5 and CoNi-ZSM5 catalysts, show only characteristic reflections of parent zeolite ZSM5 (Figure 1A). The main diffraction peaks of ion-exchanged zeolites are detected at the 2θ of $7.9, 8.8, 23.1, 23.9,$ and 24.3° , which are in the range $2\theta = 7\text{--}9^\circ$ and $23\text{--}25^\circ$ characteristic of the ZSM-5 crystal structure [19].

The characteristic diffraction peaks of starting zeolite, presented in diffractograms of all ion-exchanged samples, reveal that the structure of ZSM5 is retained after ion exchange with transition metals, and no differences in crystallinity are detected. In addition, no other phases related to Co, Ni, or Zn species were observed. These findings indicate that only a small fraction of transition metals, Co, Ni, and Zn species, is introduced by ion exchange inside the zeolite framework and it is highly dispersed.

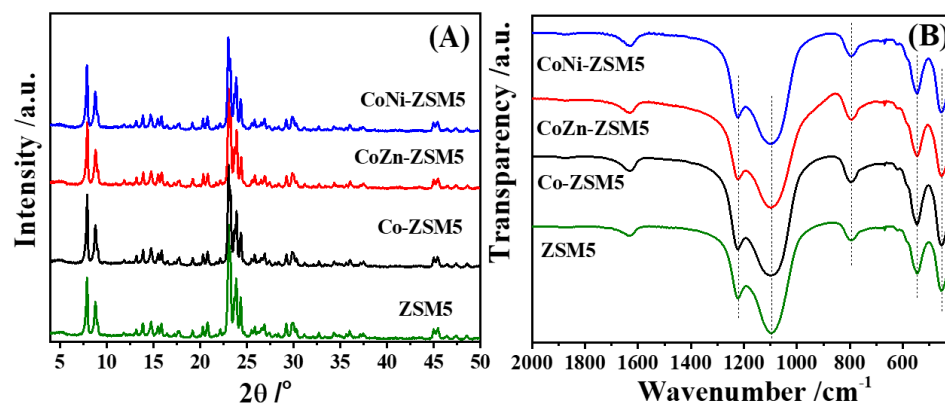


Figure 1. Diffractograms of parent and ion-exchanged ZSM-5 zeolites (A), and FTIR spectra of parent and ion-exchanged ZSM-5 zeolites (B).

The FTIR spectra of starting and ion-exchanged ZSM-5 zeolites are shown in Figure 1B. The bands characteristic for vibrations of the ZSM-5 zeolite aluminosilicate framework are present in the FTIR of starting and cation-exchanged zeolites at 453, 545, 794, 1095, and 1221 cm^{-1} , which correspond to the bending vibration of the T-O bond, external double-ring vibration, external symmetric T-O stretching vibration, T-O-T asymmetric stretching, and external T-O-T asymmetric stretching, respectively [27]. FTIR spectra do not show any evidence of perturbation of the zeolite framework due to the ion-exchange procedure, which is consistent with the XRD results. In addition, the relative bands' intensities are the same for Co-ZSM5, CoZn-ZSM5, and CoNi-ZSM5.

The N_2 adsorption–desorption isotherms and pore distribution of starting and ion-exchanged ZSM-5 zeolites are presented in Figure 2. Also, the BET surface area and pore structure results of all synthesized samples are summarized in Table 1. All investigated zeolites showed typical type I isotherms corresponding to microporous materials [28]. A little influence of the ion-exchange procedure on the textural properties was confirmed by the investigation of the obtained results (Table 1) because all N_2 adsorption–desorption isotherms were similar to each other. This finding is in accordance with the XRD and FTIR spectroscopy results.

However, a slight decrease in the BET surface area was detected for both Co-ZSM5 and CoZn-ZSM5 zeolites. This finding could have originated from pore blocking, which might have occurred due to cobalt and/or zinc species either dispersed in the channels or deposited on the outer surface of the zeolite. The microporous volume was not affected by the ion-exchange procedure, demonstrating the preservation of the structure of the investigated zeolites.

Total pore volume slightly increased after the introduction of metals in the ZSM-5 zeolite, indicating some surface mesoporosity.

The representative results obtained by the SEM-EDS analysis of the investigated electrocatalysts are presented in Figure 3. SEM micrographs show that all metal-exchanged electrocatalysts have a close resemblance or identical morphologies. This finding is in accordance with the results obtained by other applied characterization techniques, XRD, FTIR spectroscopy, and low-temperature nitrogen adsorption; namely, the structural and textural characteristics of the parent ZSM-5 zeolite were not significantly affected by the ion-exchange procedure.

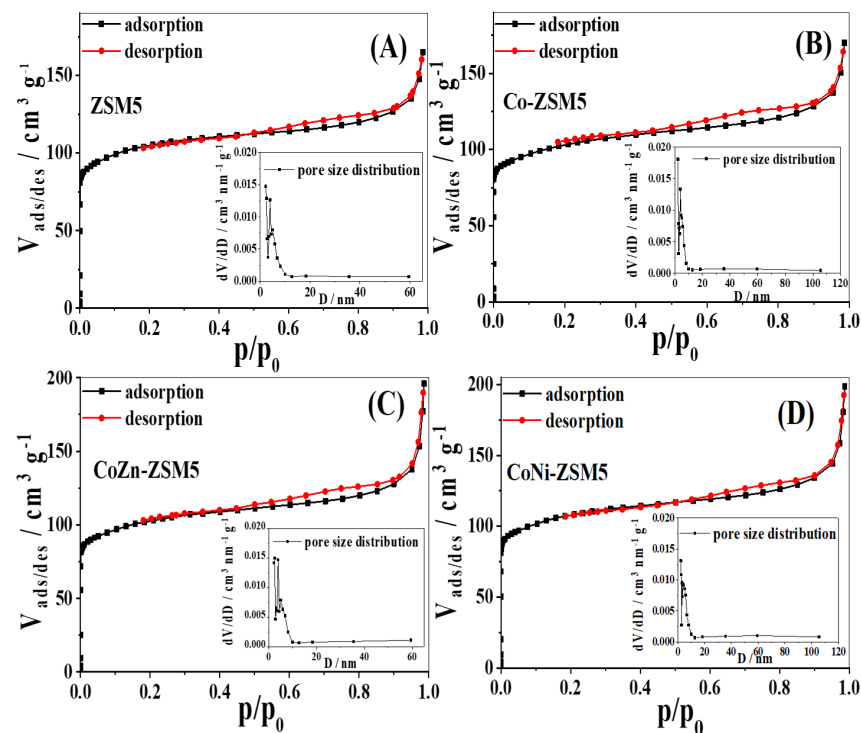


Figure 2. Nitrogen adsorption-desorption isotherms of parent and ion-exchanged ZSM-5 zeolites.

Table 1. Zeolite's textural properties obtained by BET analysis and t-plot methods.

Sample	S_{BET}^a m^2/g	S_{external}^b m^2/g	V_{micro}^c cm^3/g	V_{tot}^d cm^3/g
ZSM5	349	40	0.147	0.255
Co-ZSM5	344	45	0.142	0.303
CoZn-ZSM5	342	46	0.142	0.263
CoNi-ZSM5	360	54	0.145	0.307

^a S_{BET} —specific surface area calculated using the Brunauer–Emmett–Teller (BET) method from N_2 isotherms.

^b S_{external} —calculated by t-plot ($t \approx 0.5$ – 0.75). ^c V_{micro} —micropore volume, calculated by t-plot ($t \approx 0.5$ – 0.75).

^d V_{tot} —total pore volume calculated from the desorption isotherm at $P/P_0 = 0.985$.

Chemical compositions, shown in Table 2, determined on the surface of investigated electrocatalysts by EDS analysis show that low amounts of transition metals were introduced into the zeolitic structure (about 1 wt%). The amount of Co introduced during the first ion-exchange procedure does not seem to be affected by an additional ion-exchange cycle with Zn or Ni cations.

Table 2. Elemental compositions detected on the surface of investigated zeolites by EDS analysis.

Element	ZSM5	Co-ZSM5	CoZn-ZSM5	CoNi-ZSM5
	wt %			
O	57.94 ± 0.35	54.59 ± 0.37	58.65 ± 0.40	55.10 ± 0.27
Si	39.51 ± 0.33	42.57 ± 0.34	37.88 ± 0.36	41.75 ± 0.25
Al	2.55 ± 0.10	2.54 ± 0.09	2.52 ± 0.11	2.71 ± 0.07
Co		0.27 ± 0.13	0.24 ± 0.14	0.25 ± 0.09
Zn			0.71 ± 0.23	
Ni				0.20 ± 0.19

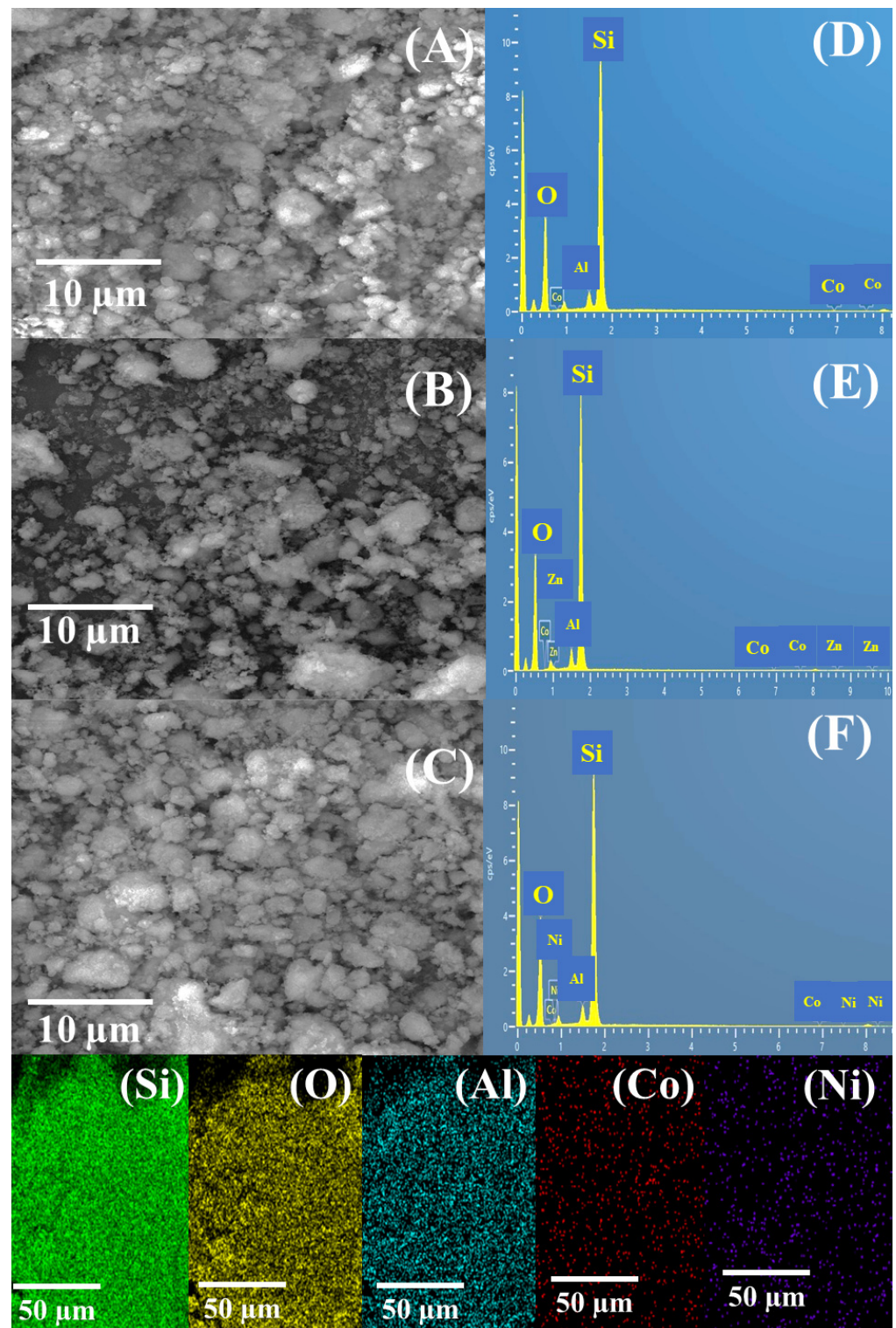


Figure 3. SEM micrographs of Co-ZSM5 (A), CoZn-ZSM5 (B), and CoNi-ZSM5 (C) with the corresponding EDS spectra of Co-ZSM5 (D), CoZn-ZSM5 (E), and CoNi-ZSM5 (F), and the elemental mapping of CoNi-ZSM5.

3.2. Oxygen Evolution Reaction Investigation

Figure 4 shows cyclic voltammograms (CVs) obtained in an N_2 -saturated solution for three studied zeolites recorded in the non-Faradaic potential region at different scan rates [13,16]. These results (Figure 4D) are used for the calculation of the double-layer capacitance (C_{dl})

that is directly proportional to the electrochemical active surface area (ECSA) [13,16]. C_{dl} values were found to be of the same order of magnitude, though somewhat higher in the case of Co-ZSM5 (2.8 mF cm^{-2}) of CoZn-ZSM5 (1.6 mF cm^{-2}) and CoNi-ZSM5 (1.6 mF cm^{-2}) electrodes, implying a somewhat higher ECSA and number of active sites for OERs in the case of Co-ZSM5 [29]. Still, the accessibility and oxidation state of the active sites play an important role in the material's activity for the OERs, so a higher ECSA/number of active sites does not always lead to higher current densities [13,30–33]. Moreover, some studies emphasize the fact that a non-Faradaic C_{dl} was obtained by measuring the current density due to electrolytes' adsorption/desorption, while the OER current was obtained due to electron transfer, which is a clear Faradaic process [29].

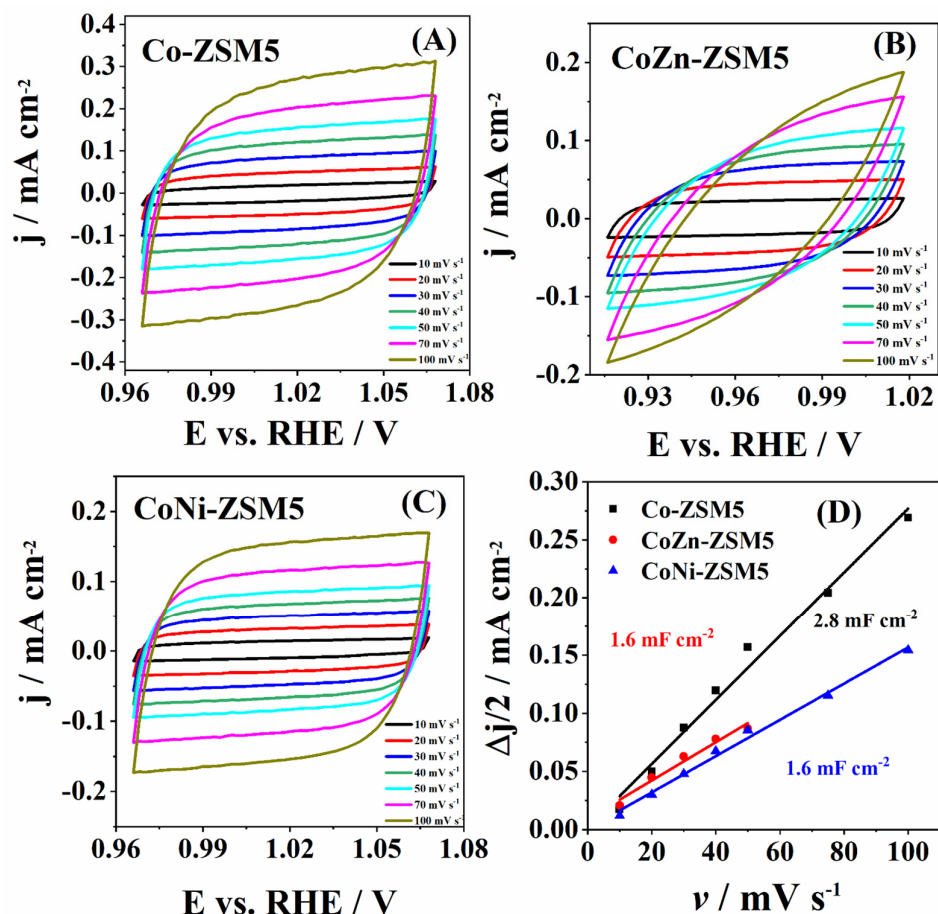


Figure 4. CVs of Co-ZSM5 (A), CoZn-ZSM5 (B), and CoNi-ZSM5 (C) in an N₂-saturated 1 M KOH solution at different scan rates ranging from 10 to 100 mV s⁻¹ with the corresponding double-layer capacitance plots (D).

The activities of Co-ZSM5, CoZn-ZSM5, and CoNi-ZSM5 toward OER catalysis were next investigated by LSV in alkaline media (Figure 5A). An onset potential (E_{onset}) of 1.61 V was observed for both CoNi-ZSM5 and Co-ZSM5 and a 30 mV higher value for CoZn-ZSM5 (1.64 V). Accordingly, the corresponding overpotential (η_{onset}) at onset potential was found to be 410 mV for both CoNi-ZSM5 and Co-ZSM5 and 440 mV for CoZn-ZSM5. The overpotential value determined for CoNi-ZSM5 and Co-ZSM5 was equivalent to that of calcined Ce- β (410 mV), but was 110 mV lower than that of Ce- β (520 mV) (Table 3) [16]. Furthermore, the η_{onset} value was 80 and 50 mV lower compared to Ce-ZSM-5 (480 mV) and Ce-ZSM-5 cal (460 mV), respectively [16]. Similarly, synthetic 13X and natural clinoptilolite exchanged with Ce (Ce-Cl_i, Ce-Cl_i cal, and Ce-13X) showed values of η_{onset} 60 to 120 mV higher than the CoNi-ZSM5 and Co-ZSM5 in this study [13]. The only exception was Ce-13X cal, with a comparable η_{onset} of 400 mV [13].

CoNi-ZSM5 reached the highest current density of 9.5 mA cm^{-2} , followed by Co-ZSM5 (6.8 mA cm^{-2}), while CoZn-ZSM5 showed the lowest current density of 2.3 mA cm^{-2} at 2 V (Figure 5A).

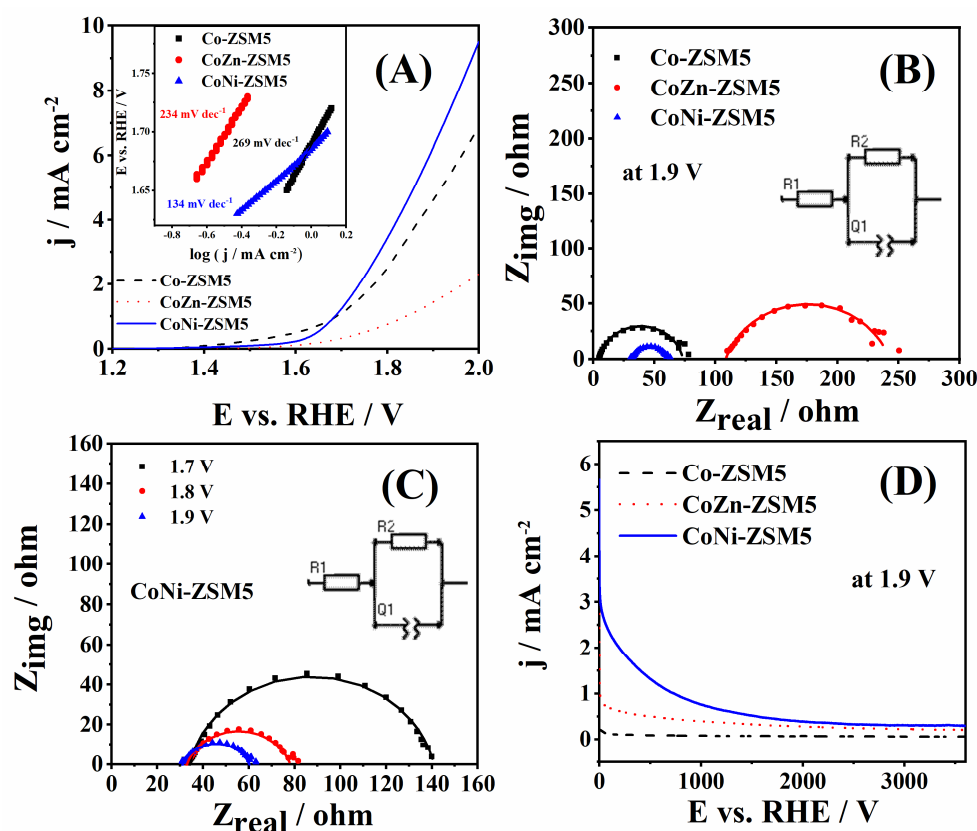


Figure 5. Polarization curves (iR -corrected) of Co-ZSM5, CoZn-ZSM5, and CoNi-ZSM5 at 20 mV s^{-1} , with the corresponding Tafel plots in the inset (A); Nyquist plots of three CoM-ZSM5 electrodes at -1.9 V (B) and of CoNi-ZSM5 at three different potentials (1.7, 1.8, and 1.9 V), with the corresponding equivalent circuit used to fit the experimental data; (C) and chronoamperometric curves of CoM-ZSM5 electrodes at 1.9 V at 3600 s (D) in a 1 M KOH solution.

Table 3. Kinetic parameters of OER at Co-ZSM5, CoZn-ZSM5, and CoNi-ZSM5 compared with those of similar zeolite electrodes from the literature reports.

OER Electrocatlysts	$E_{\text{onset}}/\text{V}$	$\eta_{\text{onset}}/\text{mV}$	$b/\text{mV dec}^{-1}$	j at 2 V/ mA cm^{-2}	References
Co-ZSM5	1.61	410	269	6.8	This work
CoZn-ZSM5	1.64	440	234	2.3	This work
CoNi-ZSM5	1.61	410	134	9.5	This work
Ce-ZSM-5	1.68	480	207	1.6	[16]
Ce-ZSM-5 cal	1.66	460	202	1.7	[16]
Ce- β	1.72	520	312	2.6	[16]
Ce- β cal	1.61	410	114	7.3	[16]
Ce- Cl_i	1.73	530	220	1.2	[13]
Ce- Cl_i cal	1.69	490	278	1.54	[13]
Ce-13X	1.67	470	280	2.14	[13]
Ce-13X cal	1.60	400	296	4.6	[13]

Table 3. Cont.

OER Electrocatalysts	$E_{\text{onset}}/\text{V}$	$\eta_{\text{onset}}/\text{mV}$	$b/\text{mV dec}^{-1}$	j at 2 V/mA cm^{-2}	References
NiA	/	/	463	~13	[11]
NiX	/	/	842	~3	[11]
Co ₃ O ₄ /NCN	/	~380	102	/	[34]
Co-O@HNC	/	/	105.7	/	[35]
CoRu-A@HNC	/	/	180.6	/	[35]
Co@NC	/	/	90	/	[36]
Co ₃ O ₄ @NCNs	/	/	220	/	[36]
CoPt/mpg-CN	1.62	/	160	/	[37]
CoPt/C (46.7 wt% Pt)	1.59	/	208	/	[37]

Tafel slopes of 134, 234, and 269 mV dec^{-1} were determined for CoNi-ZSM5, CoZn-ZSM5, and Co-ZSM5 respectively (Figure 5A inset). CoNi-ZSM5 showed the lowest value of the Tafel slope reflecting the highest rate of OER in this zeolite. These values are comparable with different types of zeolites exchanged with Ce [13,16]. On the other hand, Ce- β , Ce-Clical, and Ce-13X cal presented higher Tafel slopes than all the zeolites examined in this study [13,16]. Tafel slope values as high as 842 and 463 mV dec^{-1} were obtained for OERs of NiX and NiA zeolites, significantly higher than the values presented in this study [11]. Moreover, the Tafel slope value evaluated for CoNi-ZSM5 was comparable to that of OER electrocatalysts of different classes of materials. For instance, the cobalt oxide compound on nitrogen-doped carbon nanosheets (Co₃O₄/NCN) tested for OER in alkaline media showed a somewhat lower Tafel slope of 102 mV dec^{-1} than CoNi-ZSM5 [34]. Co/Co₃O₄ with a small fraction of RuO₂ integrated into a hollow carbon matrix (Co-O@HNC and CoRu-A@HNC) showed Tafel slopes of 105.7 and 180.6 mV dec^{-1} , respectively, in 0.1 M KOH [35]. Defect-rich N-doped carbon nanosheets supported with Co₃O₄ nanoparticles (Co@NC and Co₃O₄@NCNs) showed high OER activity, where Tafel slopes of 90 and 220 mV dec^{-1} were calculated for Co₃O₄@NCNs and Co@NC, respectively [36]. It is interesting to note that Co₄₅Pt₅₅ alloy nanoparticles synthesized on mesoporous graphitic carbon nitride (CoPt/mpg-CN) and commercial CoPt/KB [37] showed Tafel slopes of 160 and 208 mV dec^{-1} in alkaline media during OERs, respectively. These values are higher compared to this of CoNi-ZSM5, which does not contain precious metals that directly impact the catalyst's price.

Table 4 shows the EIS parameters for Co-ZSM5, CoZn-ZSM5, and CoNi-ZSM5 electrodes obtained by fitting EIS data using an appropriate equivalent circuit (Figure 5B inset). The validity of EIS data before the fitting procedure was checked by the Kramers–Kronig validation test (KK test) [38]. The two-times-lower charge-transfer resistance, R_{ct} , was evaluated for CoNi-ZSM5 (31.5 Ω) instead of for Co-ZSM5 (68.7 Ω), which can be observed in the Nyquist plots presented in Figure 5B. The highest R_{ct} was noticed for the CoZn-ZSM5 electrode (133.4 Ω). These EIS parameters are in agreement with the OER results obtained by LSV. Figure 5C shows the Nyquist plots of the CoNi-ZSM5 electrode recorded at three different potentials. R_{ct} values of CoNi-ZSM5 of 31.5, 45.4, and 106.8 Ω were obtained at 1.9, 1.8 and 1.7 V, respectively. The R_{ct} value of CoNi-ZSM5 decreases with the increasing potential value.

CA curves of Co-ZSM5 and CoZn-ZSM5 recorded at 1.9 V showed stable current densities after the first 50 s, while the current density of CoNi-ZSM5 became constant after 1500 s during the OER. The drop in current density values partially came from the existence of oxygen bubbles covering the electrode surface and thus reducing the ECSA. Still, CoNi-ZSM5 showed the highest current density during the OER, which is in agreement with the results obtained by CV and EIS. This behavior could be a consequence of the highest BET

surface area of CoNi-ZSM5 due to the higher number of free pores than in the cases of Co and CoZn/rGO. Moreover, CoNi-ZSM5 displayed the highest pore size that assisted the mass transport to/from the electrode leaving the active sites available for fresh electrolytes.

Table 4. Electrochemical impedance spectroscopy (EIS) parameters of Co-ZSM5, CoZn-ZSM5, and CoNi-ZSM5 in 1 M KOH at 1.9 V.

Electrocatalyst	R_s (Ω)	R_{ct} (Ω)	Q_e (mF)
Co-ZSM5	4.8	68.7	6.5×10^{-4}
CoZn-ZSM5	109.3	133.4	1.1×10^{-3}
CoNi-ZSM5	29.5	31.5	6.4×10^{-4}

R_s —electrolyte resistance, R_{ct} —resistances of the charge transfer reaction, and Q_e —constant phase element.

It is well known that cobalt metal electrocatalysts have centers that are potentially active for OERs in alkaline rather than in acidic media [39]. The most investigated cobalt centers are CoO_x and CoOOH in alkaline media [39]. Density functional theory (DFT) calculations of OER pathways in cobalt-based electrocatalysts (CoCat) suggest three options [40]. The first option, the rate of H^+ mobility at the CoCat/ H_2O interface, has a direct impact on the distribution of terminal Co(III)-OH groups [39,40]. The second option shows that OERs start by releasing a proton from terminal Co-OH sites, which favor the existence of proton-acceptor species or the formation of a Co(IV)=O^\bullet oxyl radical in solution [39,40]. The third option offers the coupling of Co=O radicals with Co-OH or $\text{Co-}\mu\text{O-Co}$ species to make hydroperoxo and peroxy intermediates, which presents the irreversible chemical step where an attachment of the external water molecule to Co=O radicals is discouraged by a high-energy barrier [39,40].

4. Conclusions

Catalytic activity regarding OERs in alkaline media was exhibited by the studied Co-ZSM5, CoZn-ZSM5, and CoNi-ZSM5 electrocatalysts. The electrocatalysts, prepared by simple and inexpensive aqueous ion-exchange procedures, were characterized in detail by XRD, FTIR, SEM-EDS, and low-temperature nitrogen adsorption techniques. E_{onset} of 1.61 V was found for both CoNi-ZSM5 and Co-ZSM5 electrodes, 1.64 V for CoZn-ZSM5, a corresponding overpotential η_{onset} of 410 mV for both CoNi-ZSM5 and Co-ZSM5, and 440 mV for CoZn-ZSM5 electrodes. The highest OER current was noticed for CoNi-ZSM5, followed by Co-ZSM5, while the lowest OER current density was obtained for CoZn-ZSM5 electrocatalysts. This behavior could be the consequence of the remarkable difference in R_{ct} , where the R_{ct} of CoZn-ZSM5 is almost four-times higher than the R_{ct} of CoNi-ZSM5. Tafel slopes of 134, 234, and 269 mV dec^{-1} were observed for CoNi-ZSM5, CoZn-ZSM5, and Co-ZSM5, respectively. Finally, the highest OER activity was observed for CoNi-ZSM5, and slightly lower activity was noticed for Co-ZSM5. These CoM-ZSM5 electrodes could be good potential candidates for renewable energy devices because of their low price and stable activity during OERs.

Author Contributions: Conceptualization, J.M. and L.D.-V.; formal analysis, J.M., S.S., K.R., V.R. and L.D.-V.; funding acquisition, J.M., B.Š., and L.D.-V.; investigation, J.M., L.D.-V., K.R. and S.S.; supervision, J.M., L.D.-V. and B.Š.; validation, J.M., L.D.-V. and B.Š.; visualization, J.M. and L.D.-V.; writing—original draft, J.M. and L.D.-V.; writing—review and editing, J.M., L.D.-V. and B.Š. All authors have read and agreed to the published version of the manuscript.

Funding: The authors acknowledge the financial support from the Ministry of Science, Technological Development and Innovation of the Republic of Serbia (contract no. 451-03-65/2024-03/200146, 451-03-66/2024-03/200146, 451-03-65/2024-03/200116), as well as the Portuguese Foundation for Science and Technology (FCT, Portugal), project EXPL/EQU-EQU/0517/2021.

Data Availability Statement: Data are available upon request from the corresponding authors.

Conflicts of Interest: The authors declare no conflicts of interest. The funders had no role in the design of the study; in the collection, analyses, or interpretation of data; in the writing of the manuscript; or in the decision to publish the results.

References

1. Hanan, A.; Solangi, M.Y.; Lakhan, M.N.; Alhazaa, A.; Shar, M.A.; Laghari, A.J.; Soomro, I.A.; Abro, M.I.; Kumar, M.; Aftab, U. CoSe₂@Co₃O₄ nanostructures: A promising catalyst for oxygen evolution reaction in alkaline media. *Catal. Commun.* **2023**, *186*, 106830. [[CrossRef](#)]
2. Zhang, M.-C.; Liu, M.-Y.; Yang, M.-X.; Liu, X.-X.; Shen, S.-Y.; Wu, J.-S.; Pei, W.-B. Copper-cobalt bimetallic conductive metal-organic frameworks as bifunctional oxygen electrocatalyst in alkaline and neutral media. *J. Solid State Chem.* **2023**, *325*, 124133. [[CrossRef](#)]
3. Wang, M.; Chen, Y.; Li, T. Controllable preparation of nickel phosphide using iron and cobalt as electrocatalyst for hydrogen evolution reaction in alkaline media. *Mater. Today Chem.* **2022**, *24*, 100914. [[CrossRef](#)]
4. Park, D.H.; Kim, M.H.; Kim, M.; Byeon, J.H.; Jang, J.S.; Kim, J.H.; Lim, D.M.; Park, S.H.; Gu, Y.H.; Kim, J.; et al. Spherical nickel doped cobalt phosphide as an anode catalyst for oxygen evolution reaction in alkaline media: From catalysis to system. *Appl. Catal. B Environ.* **2023**, *327*, 122444. [[CrossRef](#)]
5. Lee, Y.; Suntivich, J.; May, K.J.; Perry, E.E.; Shao-Horn, Y. Synthesis and activities of rutile IrO₂ and RuO₂ nanoparticles for oxygen evolution in acid and alkaline solutions. *J. Phys. Chem. Lett.* **2012**, *3*, 399–404. [[CrossRef](#)] [[PubMed](#)]
6. Li, G.; Yu, H.; Song, W.; Wang, X.; Li, Y.; Shao, Z.; Yi, B. Zeolite-templated Ir_xRu_{1-x}O₂ electrocatalysts for oxygen evolution reaction in solid polymer electrolyte water electrolyzers. *Int. J. Hydrogen Energy* **2012**, *37*, 16786–16794. [[CrossRef](#)]
7. Kim, M.H.; Park, D.H.; Byeon, J.H.; Lim, D.M.; Gu, Y.H.; Park, S.H.; Park, K.W. Fe-doped Co₃O₄ nanostructures prepared via hard-template method and used for the oxygen evolution reaction in alkaline media. *J. Ind. Eng. Chem.* **2023**, *123*, 436–446. [[CrossRef](#)]
8. Du, J.; Zhang, F.; Jiang, L.; Guo, Z.; Song, H. Enhanced cobalt MOF electrocatalyst for oxygen evolution reaction via morphology regulation. *Inorg. Chem. Commun.* **2023**, *158*, 111661. [[CrossRef](#)]
9. Wu, Y.; Zang, J.; Dong, L.; Zhang, Y.; Wang, Y. High performance and bifunctional cobalt-embedded nitrogen doped carbon/nanodiamond electrocatalysts for oxygen reduction and oxygen evolution reactions in alkaline media. *J. Power Sources* **2016**, *305*, 64–71. [[CrossRef](#)]
10. Mathi, S.; Ashok, V.; Alodhayb, A.N.; Pandiaraj, S.; Shetti, N.P. Cobalt decorated S-doped carbon electrocatalyst assembly for enhanced oxygen evolution reaction. *Mater. Today Sustain.* **2024**, *26*, 100717. [[CrossRef](#)]
11. Milikić, J.; Vasić, M.; Amaral, L.; Cvjetičanin, N.; Jugović, D.; Hercigonja, R.; Šljukić, B. NiA and NiX zeolites as bifunctional electrocatalysts for water splitting in alkaline media. *Int. J. Hydrogen Energy* **2018**, *43*, 18977–18991. [[CrossRef](#)]
12. Vinodh, R.; Deviprasath, C.; Muralee Gopi, C.V.V.; Raghavendra Kummar, V.G.; Atchudan, R.; Ahamad, T.; Kim, H.-J.; Yi, M. Novel 13X Zeolite/PANI electrocatalyst for hydrogen and oxygen evolution reaction. *Int. J. Hydrogen Energy* **2020**, *45*, 28337–28349. [[CrossRef](#)]
13. Milikić, J.; Stojanović, S.; Damjanović-Vasilić, L.; Vasilić, R.; Šljukić, B. Efficient bifunctional cerium-zeolite electrocatalysts for oxygen evolution and oxygen reduction reactions in alkaline media. *Synth. Met.* **2023**, *292*, 117231. [[CrossRef](#)]
14. Li, S.; Yang, Z.; Liu, Z.; Ma, Y.; Gu, Y.; Zhao, L.; Zhou, Q.; Xu, W. Bimetal zeolite imidazolate framework derived Mo_{0.84}Ni_{0.16}-Mo₂C@NC nanosphere for overall water splitting in alkaline solution. *J. Colloid Interface Sci.* **2021**, *592*, 349–357. [[CrossRef](#)] [[PubMed](#)]
15. Ding, F.; Liu, H.; Jiang, X.; Jiang, Y.; Cheng, J.; Tu, Y.; Xiao, W.; Li, C.; Yan, X. Bimetallic zeolite imidazolium framework derived multiphase Co/HNC as pH-universal catalysts with efficient oxygen reduction performance for microbial fuel cells. *Electrochim. Acta* **2023**, *438*, 141548. [[CrossRef](#)]
16. Milikić, J.; Stojanović, S.; Damjanović-Vasilić, L.; Vasilić, R.; Rakočević, L.; Lazarević, S.; Šljukić, B. Porous cerium-zeolite bifunctional ORR/OER electrocatalysts in alkaline media. *J. Electroanal. Chem.* **2023**, *944*, 117668. [[CrossRef](#)]
17. Zhang, Q.; Zhao, X.; Miao, X.; Yang, W.; Wang, C.; Pan, Q. ZIF-L-Co@carbon fiber paper composite derived Co/Co₃O₄@C electrocatalyst for ORR in alkali/acidic media and overall seawater splitting. *Int. J. Hydrogen Energy* **2020**, *45*, 33028–33036. [[CrossRef](#)]
18. Bensafi, B.; Chouat, N.; Djafri, F. The universal zeolite ZSM-5: Structure and synthesis strategies. A review. *Coord. Chem. Rev.* **2023**, *496*, 215397. [[CrossRef](#)]
19. Baerlocher, C.; McCusker, L.B.; Olson, D.H. *Atlas of Zeolite Framework Types*, 6th ed.; Elsevier Science: Amsterdam, The Netherlands, 2007; ISBN 9780080554341.
20. Tao, Y.; Wei, W.; Gu, Q.; Jiang, X.; Li, D. Desilicated zeolite ZSM-5 based composite polymer electrolytes for solid-state lithium metal batteries. *Mater. Lett.* **2023**, *351*, 134934. [[CrossRef](#)]
21. Dong, X.; Mi, W.; Yu, L.; Jin, Y.; Lin, Y.S. Zeolite coated polypropylene separators with tunable surface properties for lithium-ion batteries. *Microporous Mesoporous Mater.* **2016**, *226*, 406–414. [[CrossRef](#)]
22. Chen, L.; Kishore, B.; Walker, M.; Dancer, C.E.J.; Kendrick, E. Nanozeolite ZSM-5 electrolyte additive for long life sodium-ion batteries. *Chem. Commun.* **2020**, *56*, 11609–11612. [[CrossRef](#)] [[PubMed](#)]

23. Xi, J.; Qiu, X.; Chen, L. PVDF-PEO/ZSM-5 based composite microporous polymer electrolyte with novel pore configuration and ionic conductivity. *Solid State Ionics* **2006**, *177*, 709–713. [[CrossRef](#)]
24. Zhang, J.; Xiang, Y.; Jamil, M.I.; Lu, J.; Zhang, Q.; Zhan, X.; Chen, F. Polymers/zeolite nanocomposite membranes with enhanced thermal and electrochemical performances for lithium-ion batteries. *J. Memb. Sci.* **2018**, *564*, 753–761. [[CrossRef](#)]
25. Smeets, P.J.; Woertink, J.S.; Sels, B.F.; Solomon, E.I.; Schoonheydt, R.A. Transition-Metal Ions in Zeolites: Coordination and Activation of Oxygen. *Inorg. Chem.* **2010**, *49*, 3573–3583. [[CrossRef](#)] [[PubMed](#)]
26. Jović, A.; Milikić, J.; Bajuk-Bogdanović, D.; Milojević-Rakić, M.; Vasiljević, B.N.; Krstić, J.; Cvjetičanin, N.; Šljukić, B. 12-phosphotungstic Acid Supported on BEA Zeolite Composite with Carbonized Polyaniline for Electroanalytical Sensing of Phenols in Environmental Samples. *J. Electrochem. Soc.* **2018**, *165*, H1013–H1020. [[CrossRef](#)]
27. Karge, H.G.; Geidel, E. *Molecular Sieves—Characterization I*; Springer: Berlin/Heidelberg, Germany, 2004; Volume 4, pp. 1–540. [[CrossRef](#)]
28. Rouquerol, F.; Rouquerol, J.; Sing, K. Assessment of Mesoporosity. In *Adsorption by Powders and Porous Solids*; Elsevier: Amsterdam, The Netherlands, 1999; pp. 191–217.
29. Anantharaj, S.; Sugime, H.; Noda, S. Why shouldn't double-layer capacitance (C_{dl}) be always trusted to justify Faradaic electrocatalytic activity differences? *J. Electroanal. Chem.* **2021**, *903*, 115842. [[CrossRef](#)]
30. Stevens, M.B.; Enman, L.J.; Batchellor, A.S.; Cosby, M.R.; Vise, A.E.; Trang, C.D.M.; Boettcher, S.W. Measurement techniques for the study of thin film heterogeneous water oxidation electrocatalysts. *Chem. Mater.* **2017**, *29*, 120–140. [[CrossRef](#)]
31. Klingan, K.; Ringleb, F.; Zaharieva, I.; Heidkamp, J.; Chernev, P.; Gonzalez-Flores, D.; Risch, M.; Fischer, A.; Dau, H. Water oxidation by amorphous cobalt-based oxides: Volume activity and proton transfer to electrolyte bases. *ChemSusChem* **2014**, *7*, 1301–1310. [[CrossRef](#)]
32. Jung, S.; McCrory, C.C.L.; Ferrer, I.M.; Peters, J.C.; Jaramillo, T.F. Benchmarking nanoparticulate metal oxide electrocatalysts for the alkaline water oxidation reaction. *J. Mater. Chem. A* **2016**, *4*, 3068–3076. [[CrossRef](#)]
33. Doyle, R.L.; Godwin, I.J.; Brandon, M.P.; Lyons, M.E.G. Redox and electrochemical water splitting catalytic properties of hydrated metal oxide modified electrodes. *Phys. Chem. Chem. Phys.* **2013**, *15*, 13737–13783. [[CrossRef](#)]
34. Wang, H.; Yang, P.; Sun, X.; Xiao, W.; Wang, X.; Tian, M.; Xu, G.; Li, Z.; Zhang, Y.; Liu, F.; et al. Co-Ru alloy nanoparticles decorated onto two-dimensional nitrogen doped carbon nanosheets towards hydrogen/oxygen evolution reaction and oxygen reduction reaction. *J. Energy Chem.* **2023**, *87*, 286–294. [[CrossRef](#)]
35. Li, G.; Zheng, K.; Li, W.; He, Y.; Xu, C. Ultralow Ru-Induced Bimetal Electrocatalysts with a Ru-Enriched and Mixed-Valence Surface Anchored on a Hollow Carbon Matrix for Oxygen Reduction and Water Splitting. *ACS Appl. Mater. Interfaces* **2020**, *12*, 51437–51447. [[CrossRef](#)] [[PubMed](#)]
36. Xi, W.; Shen, M.; Yin, X.; Gao, B.; He, L.; Chen, Y.; Lin, B. Molten-salt confined synthesis of nitrogen-doped carbon nanosheets supported Co_3O_4 nanoparticles as a superior oxygen electrocatalyst for rechargeable Zn-air battery. *J. Power Sources* **2023**, *560*, 232692. [[CrossRef](#)]
37. Andrić, S.; Milikić, J.; Sevim, M.; Santos, D.M.F.F.; Šljukić, B. Effect of carbon support on the activity of monodisperse $\text{Co}_{45}\text{Pt}_{55}$ nanoparticles for oxygen evolution in alkaline media. *Front. Chem.* **2023**, *11*, 1244148. [[CrossRef](#)] [[PubMed](#)]
38. Bastidas, D.M.; Cano, E. Validation of titanium corrosion impedance data using Kramers–Kronig relationships. *Surf. Eng.* **2006**, *22*, 384–389. [[CrossRef](#)]
39. Zhong, H.; Campos-Roldán, C.A.; Zhao, Y.; Zhang, S.; Feng, Y.; Alonso-Vante, N. Recent advances of cobalt-based electrocatalysts for oxygen electrode reactions and hydrogen evolution reaction. *Catalysts* **2018**, *8*, 559. [[CrossRef](#)]
40. Mattioli, G.; Giannozzi, P.; Amore Bonapasta, A.; Guidoni, L. Reaction pathways for oxygen evolution promoted by cobalt catalyst. *J. Am. Chem. Soc.* **2013**, *135*, 15353–15363. [[CrossRef](#)]

Disclaimer/Publisher's Note: The statements, opinions and data contained in all publications are solely those of the individual author(s) and contributor(s) and not of MDPI and/or the editor(s). MDPI and/or the editor(s) disclaim responsibility for any injury to people or property resulting from any ideas, methods, instructions or products referred to in the content.